RSC Advances

PAPER

View Article Online
View Journal | View Issue

Cite this: *RSC Adv.*, 2017, **7**, 19205

Hexagonal β-Na(Y,Yb)F_4 based core/shell nanorods: epitaxial growth, enhanced and tailored up-conversion emission†

Jing Yan,[a] Honghu Yao,[a] Junhao Li,[a] Shiman He,[a] Qili Wu,[a] Xianfeng Yang,[b] Wasim Ullah Khan,[a] Jianxin Shi*[a] and Mingmei Wu*[a]

Received 12th January 2017
Accepted 18th March 2017

DOI: 10.1039/c7ra00475c

rsc.li/rsc-advances

To meet the increasing requirement, much effort has been devoted to enhance the emission intensity and tailor the emission color of rare earth phosphors. However, limited contributions have been made to the up-conversion (UC) of nanorods by complete epitaxial growth on each facet to achieve this requirement. In this study, we propose a facile epitaxial growth route to grow anisotropic hexagonal β-$NaYF_4$:Yb^{3+}/Ho^{3+}@β-$NaYbF_4$:Er^{3+}, β-$NaYF_4$:Yb^{3+}/Ho^{3+}@β-$NaYF_4$, and β-$NaYbF_4$:Er^{3+}@β-$NaYF_4$ core/shell nanorods, which were realized by adding hexagonal β-$NaYF_4$:Yb^{3+}/Ho^{3+} or β-$NaYbF_4$:Er^{3+} nanorods as a core-nanostructure into a solution containing cubic α-$NaYbF_4$:Er^{3+} or α-$NaYF_4$ nanoparticles as the shell-precursor. During epitaxial growth-induced phase transformation, the precursor nanoparticles disappeared gradually in the solution and consequently corresponding β-phased shell yielded on each outer facet of each β-phased nanorod core. Eventually, the nanorod core was covered completely with a uniformly grown β-$NaYbF_4$:Er^{3+} or β-$NaYF_4$ shell. The UC emission of either β-$NaYF_4$:Yb^{3+}/Ho^{3+} or β-$NaYbF_4$:Er^{3+} core can be enhanced by the outer shell due to the decrease in the number of surface defects. In addition, tailored UC emissions could be obtained by controlling the shell components and thickness, typically in the core/shell nanorods of β-$NaYF_4$:Yb^{3+}/Ho^{3+}@β-$NaYbF_4$:Er^{3+}. The tunable colors with improved emission in these core/shell nanorods may find wider applications in multicolor labeling and anti-counterfeiting.

1. Introduction

Lanthanide-doped fluoride-based UC nanoparticles have received considerable attention in recent years due to their advantages, such as low autofluorescence, deep penetration with near-infrared (NIR) irradiation, high photo-stability, good chemical stability, and low cytotoxicity.[1–4] Therefore, a wide range of studies have been taken to synthesize controllable morphologies and tunable sizes of nano-/microstructured UC crystals to find potential applications, such as sensors, infrared anti-counterfeiting labeling, biological labeling, imaging and drug delivery.[5–13] Typically, the serious background noise resulting from the light excitation sources, ranging from ultra-violet to visible, limits the wide applications of down-conversion materials in the anti-counterfeiting field, while the lanthanide-doped UC materials excited by infrared light can eliminate such disadvantages.[14,15] The lanthanide-doped UC phosphors with particular nanostructures and UC colors can further strengthen anti-counterfeiting.[16]

$NaYF_4$ is regarded as one of the most effective UC luminescence matrices due to its low phonon energy (<400 cm^{-1}). In addition, hexagonal β-$NaYF_4$ always exhibits higher UC efficiency than cubic α-$NaYF_4$.[17–19] Recently, more and more efforts have been devoted to the growth of the shell on $NaYF_4$ nanocrystals.[20–22] It was reported that the coating shell can enhance the optical intensity of the core by minimizing the surface defects and consequently surface quenching. Furthermore, core/shell nanostructures can eliminate deleterious cross-relaxation between the activators, which are separated inside the different layers.[23] To date, most of the studies have focused on sphere-like $NaYF_4$ core nanocrystals with diameters ranging from 6 to 50 nm.[1,5,8,24–28] However, the surface energies are not equal on different crystal faces for non-spherical crystals, and thus coating shells on larger sized or non-spherical crystals still needs further exploration. Recently, several studies have focused on synthesizing $NaYF_4$ core-based core/shell nanorods with some oxides. For example, functional β-$NaYF_4$@SiO_2@mSiO_2 core/shell nanorods have been developed in Zhao's group.[3] Organic moieties, biomacromolecules and even nanoparticles can be grafted on the mesoporous silica shells to meet the applications in photo-inducing reaction, light-operated switch, multiple light

[a]*MOE Key Laboratory of Bioinorganic and Synthetic Chemistry, Key Laboratory of Environment and Energy Chemistry of Guangdong Higher Education Institutes, School of Chemistry, Sun Yat-Sen University, Guangzhou 510275, P. R. China. E-mail: cessjx@mail.sysu.edu.cn; ceswmm@mail.sysu.edu.cn; Tel: +86 20 8411 2830; +86 20 8411 1823*

[b]*Analytical and Testing Center, South China University of Technology, Guangzhou 510640, P. R. China*

† Electronic supplementary information (ESI) available. See DOI: 10.1039/c7ra00475c

responses, and so on. β-$NaYF_4$@TiO_2 nanorods have been grown to show enhanced photocatalytic activity under near-infrared irradiation.[29] However, both SiO_2 and TiO_2 shells are optically inert and can be coated easily on the core surface by hydrolysis. Selective epitaxial growth on specific crystal planes of disk-like and rod-like β-$NaYF_4$ have been proposed to realize multicolor UC emissions in single-particle level for anti-counterfeiting and multiplexed labeling applications.[16,30] To the best of our knowledge, the growth of optically active shell completely covering β-$NaYF_4$ or other related $NaReF_4$ (Re = rare earth) nanorods in solution using α-$NaYF_4$ nanoparticles as a shell precursor has never been reported.

In this article, shell-active β-$NaYF_4$:Yb^{3+}/Ho^{3+}@β-$NaYbF_4$:Er^{3+}, and shell-inert β-$NaYF_4$:Yb^{3+}/Ho^{3+}@β-$NaYF_4$ and β-$NaYbF_4$:Er^{3+}@β-$NaYF_4$ core/shell nanorods with a high reaction yield were synthesized *via* a facile hydrothermal method in the oleic acid–ethanol–deionized water system. The phase, morphology and core/shell nanostructure were characterized *via* X-ray powder diffraction (XRD), scanning electronic microscopy (SEM) and transmission electron microscopy (TEM), respectively. The UC emission of β-$NaYF_4$:Yb^{3+}/Ho^{3+} can be enhanced by coating either an optically active β-$NaYbF_4$:Er^{3+} or an inert β-$NaYF_4$ shell due to the surface passivation effect. In this way, with a coating of the inert β-$NaYF_4$, the red emission of β-$NaYbF_4$:Er^{3+} can also be improved. Tunable colors in the core/shell nanorods can be observed and they may find potential applications in multicolor labeling and anti-counterfeiting.

2. Experimental

2.1 Materials

Yttrium nitrate hexahydrate (99.9%) and ytterbium nitrate pentahydrate (99.9%) were purchased from Aladdin Reagents. Er_2O_3 (99.9%) and Ho_2O_3 (99.9%) were provided by Guangzhou Zhujiang Rare Earths Co., Ltd. and dissolved in dilute HNO_3 under heating to prepare the $Er(NO_3)_3$ and $Ho(NO_3)_3$ solutions. Sodium hydroxide (NaOH, > 98%) and ammonium fluoride (NH_4F, > 98%) were purchased from Guangzhou Chemical Reagent Factory. Ethanol (A.R.) and oleic acid (90%) were purchased from Tianjin Damao Chemical Reagent Factory. All the chemical reagents used in this experiment were received without further purification. Deionized (DI) water was used throughout.

2.2 Preparation

The preparation of the core nanorods. The β-$NaReF_4$ nanorods were synthesized by a slightly modified literature procedure *via* a facile hydrothermal reaction.[16] In a typical experiment, 5 mL oleic acid and 5 mL ethanol were first added to a 25 mL Teflon lining with vigorous stirring. Second, 1.5 mL DI water containing 7.5 mmol NaOH was added, followed by the addition of 1 mL NH_4F (2 mol L^{-1}) solution. Subsequently, 1 mL aqueous solution of $Re(NO_3)_3$ (0.4 mol L^{-1}, Re = Y, Yb, Er and/or Ho at a certain percentage) was added. The final solution was kept stirring for another 30 min. The Teflon cup containing the resulting mixture solution was closed tightly and kept inside a stainless steel autoclave and the autoclave was transferred into an oven where it was then heated to 220 °C for 24 h. As the autoclave was cooled naturally to room temperature, the precipitates were separated by centrifugation, washed 5 times with DI water and ethanol, and finally dried in air at 70 °C for 12 h.

The synthesis of the shell precursor. The α-$NaReF_4$ nanoparticles were synthesized using the same procedure as that for β-$NaReF_4$ except for reaction temperature at 180 °C and reaction time of 1–4 h. After the reaction, the product was either purified for characterization or kept inside the autoclave with the mother liquid without further separation for the subsequent epitaxial growth.

The epitaxial growth of the shell on β-$NaReF_4$ nanorods. A specific volume of α-$NaReF_4$ nanoparticles, as shell precursor obtained for 2 h as described in the last paragraph, was poured into a 40 mL Teflon cup with vigorous stirring. Subsequently, one batch of the isolated β-$NaReF_4$ nanorods, as described in the first paragraph in this section, was transferred into 4 mL ethanol and dispersed under ultrasonic irradiation for 10 min. The uniformly dispersed β-$NaReF_4$ nanorods serving as core nanostructures were added dropwise into the 40 mL Teflon cup, which was kept stirring for another 30 min. The Teflon cup with a mixture of the β-phased nanorods, as core template, and the α-phased nanoparticles, as shell precursor, was then placed into an autoclave and heated at 220 °C for 12 h. As the autoclave was cooled naturally to room temperature, the precipitates were separated by centrifugation, washed 5 times with DI water and ethanol for, and then dried in air at 70 °C for 12 h. Each core template and shell precursor are denoted as the Q, P and R series. For the Q1-5 and P1-5 samples, the cores were β-$NaYF_4$:0.20Yb^{3+}, 0.02Ho^{3+} nanorods, while the shell precursors were 4, 8, 12, 16 and 20 mL of α-$NaYbF_4$:0.02Er^{3+}, and α-$NaYF_4$ nanoparticles, respectively. For the R1-5 samples, the cores were β-$NaYbF_4$:0.02Er^{3+} nanorods and the shell precursors were 4, 8, 12, 16 and 20 mL of α-$NaYF_4$ colloid solutions.

2.3 Measurements

Structural characterization. To investigate the phase purity, samples were checked by X-ray powder diffraction (XRD) using a D8 ADVANCE diffractometer with Cu Kα radiation (λ = 0.154056 nm) at room temperature (RT). A step size of 0.02° was used with a scanning speed of 10° min^{-1} in 2θ degree. The scanning electron micrograph (SEM) was obtained using a FEI Quanta scanning electron microscope operated at 20 kV. Transmission electron microscopy (TEM) was performed on a JEOL JEM-2100 transmission electron microscope operated at 200 kV.

Up-conversion luminescence. The luminescence spectra were measured with Edinburgh Instruments FLS 920 equipped with a 5 W 980 nm laser diode.

3. Results and discussion

3.1 Cubic α-$NaYbF_4$:0.02Er^{3+} shell precursor and hexagonal β-$NaYF_4$:0.20Yb^{3+}, 0.02Ho^{3+} core template

The phase purity of the cubic α-$NaYbF_4$:0.02Er^{3+} obtained under 180 °C was confirmed by powder XRD. The samples displayed distinctively different XRD patterns at different reaction

periods, as shown in Fig. S1.† The hydrothermal reactions for 1–4 h led to the formation of a pure cubic α phase. Weak diffraction peaks of its dynamically stable hexagonal β-$NaYbF_4$ appeared after prolonging the reaction time to 6 h, and the peaks became more significant with longer reaction times.

The sample of α-$NaYbF_4$:0.02Er^{3+} obtained for 2 h will be chosen as a typical shell precursor to build core/shell nanorods. The monodispersed cube-like nanoparticles around 18 nm in size can be identified by TEM images (Fig. 1a and c). Selected area electron diffraction (SAED) image (Fig. 1b) and the typical high-resolution transmission electron microscopy (HRTEM) image (Fig. 1d) indicate their good crystallization.

Pure hexagonal β-$NaYF_4$:0.20Yb^{3+}, 0.02Ho^{3+} was achieved by reacting 24 h under 220 °C (Fig. 2a). The morphology was investigated through SEM, as shown in Fig. 2b and uniform nanorods were observed with a length and diameter of *ca.* 1.5 μm and 150 nm, respectively. Fig. 2c displays a TEM image of one as-isolated β-$NaYF_4$:0.20Yb^{3+}, 0.02Ho^{3+} nanorod combined with its selected-area electron diffraction (SAED) patterns (Fig. 2d), confirming its single-crystalline nature and growth behaviour along ⟨001⟩ direction.

3.2 β-$NaYF_4$:Yb^{3+}/Ho^{3+}@β-$NaYbF_4$:Er^{3+} core/shell architecture

After epitaxial growth, as described in the experimental section, no trace of α-$NaYbF_4$ phase was detected by XRD, confirming that the α-$NaYbF_4$:0.02Er^{3+} precursor had transformed completely into β-$NaYbF_4$:0.02Er^{3+} (Fig. S2†). In order to study the present state of the resultant β-$NaYbF_4$:0.02Er^{3+}, TEM was taken into account to identify the nanostructures of Q samples obtained with different contents of the α-$NaYbF_4$:0.02Er^{3+} precursor. Fig. 3a shows a scanning transmission electron microscopy (STEM) image of a single rod of Q1 sample (the component of Q samples was described in the experimental section) under high-angle annular dark-field (HAADF). The contrast between the core (dark) and shell (bright) is clearly distinguishable. The contrast can be attributed to the much larger atomic number of Yb ($Z = 70$) compared with Y ($Z = 39$).[24] Considering the clearly different Yb^{3+} concentrations between β-$NaYF_4$:0.20Yb^{3+}, 0.02Ho^{3+} and $NaYbF_4$:0.02Er^{3+}, we can imagine that the much higher Yb^{3+} concentration sample, *i.e.* $NaYbF_4$:0.02Er^{3+}, has become the shell to cover the β-$NaYF_4$:0.20Yb^{3+}, 0.02Ho^{3+} nanorod with a lower Yb^{3+} component inside the core. To validate our hypothesis, we further measured the element mappings of Yb^{3+} and Y^{3+} for the specific nanorod, as presented in Fig. 3b–d. The distribution of Yb^{3+} and

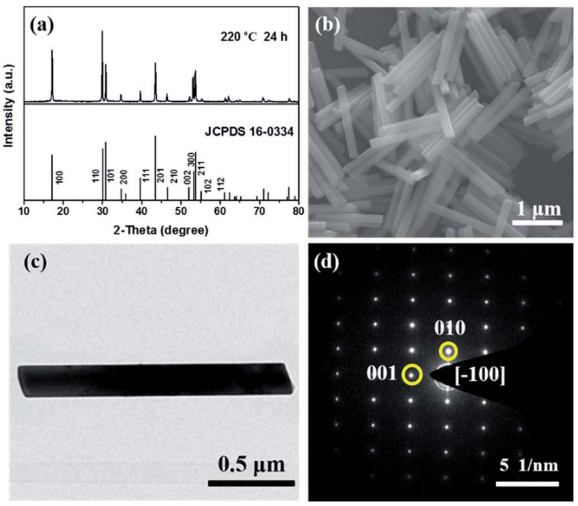

Fig. 2 (a) XRD pattern, (b) SEM image, (c) TEM image of the as-synthesized β-$NaYF_4$:0.20Yb^{3+}, 0.02Ho^{3+} and (d) the SAED of the whole nanorod in TEM image.

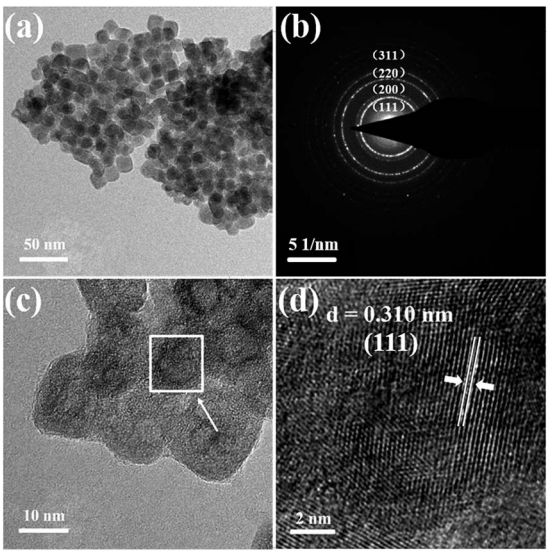

Fig. 1 TEM images (a, c), SAED analysis (b) and HRTEM image (d) of α-$NaYbF_4$:0.02Er^{3+} under 180 °C by hydrothermal treatment. HRTEM image were taken from the square region in (c). Legible lattice distance of 0.310 nm which matches well with the (111) crystal plane of α-$NaYF_4$. In addition, the typical SAED further confirmed the formation of pure α-$NaYF_4$ phase.

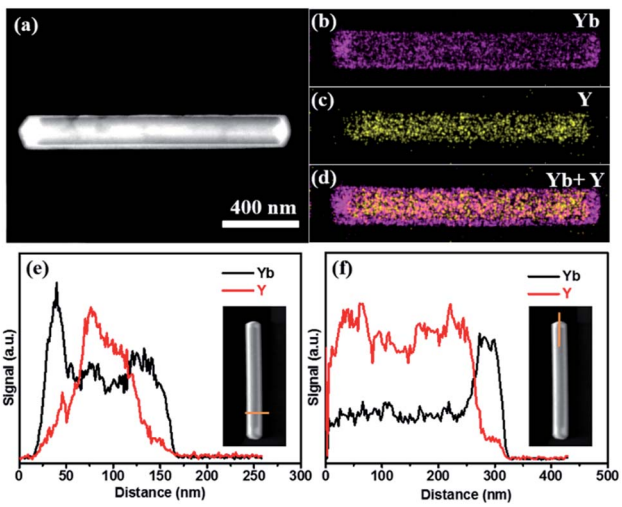

Fig. 3 (a) Typical STEM in HAADF of Q1, (b) element mapping of Yb, (c) Y and (d) Yb + Y in the rod. Corresponding EELS line scan conducted through the cross section (e) and tip (f).

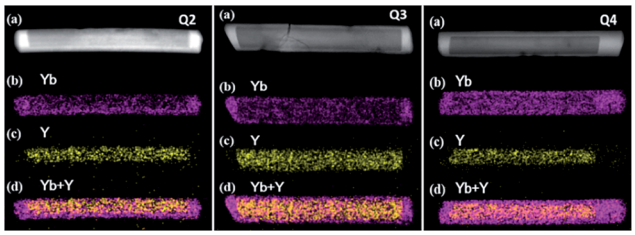

Fig. 4 (a) Typical STEM in HAADF, (b) element mapping of Yb, (c) Y and (d) Yb + Y in the rod of Q2–Q4.

Y^{3+} shows that the core/shell nanostructure was formed. The corresponding EELS line scan analyses (Fig. 3e and f) revealed a higher Yb^{3+} component on the edge of the nanorod, which is consistent with the results of element mappings and further confirms the core/shell nanoarchitecture. In addition, the element mappings of Yb^{3+} and Y^{3+} for other Q samples are shown in Fig. 4. The coverage of Yb^{3+} on Y^{3+} becomes more significant and the shell becomes thicker with increasing volume of the precursor content. The abovementioned results indicate that the optically active α-$NaYbF_4$:0.02Er^{3+} precursor changes successfully to β-$NaYbF_4$:0.02Er^{3+} and consequently grows onto β-$NaYF_4$:0.20Yb^{3+}, 0.02Ho^{3+} core nanorods with epitaxial growth behavior due to the isostructure between hexagonal β-$NaYbF_4$ and β-$NaYF_4$.

Based on the abovementioned results, the formation of hexagonal β-$NaYF_4$:Yb^{3+}/Ho^{3+}@β-$NaYbF_4$:Er^{3+} core/shell nanorods is shown in Scheme 1. First, the uniformly dispersed β-$NaYF_4$:Yb^{3+}/Ho^{3+} nanorods were mixed with α-$NaYbF_4$:Er^{3+} nanoparticles in the mother liquid. Second, the mixture of the β-phased nanorods as the core template and the α-phased nanoparticles as shell precursor in Teflon cup was then transferred to an autoclave and heated at 220 °C for 12 h. Third, during epitaxial growth-induced phase transformation, the precursor nanoparticles gradually disappeared in the solution and consequently corresponding β-phased shell yielded on each outer facet of each β-phased nanorod core. Eventually, the nanorod core was completely covered with uniformly grown β-$NaYbF_4$:Er^{3+} shell.

3.3 β-$NaYF_4$:Yb^{3+}/Ho^{3+}@β-$NaYbF_4$:Er^{3+} core/shell architecture

First, a comparison about UC emissions among lonely β-$NaYF_4$:Yb^{3+}/Ho^{3+}, β-$NaYbF_4$:Er^{3+} and core/shell nanostructured β-$NaYF_4$:Yb^{3+}/Ho^{3+}@β-$NaYbF_4$:Er^{3+} was made under 980 nm laser (0.2 W mm^{-2}) excitation at ambient temperature to investigate the effect of the shell structure on the UC luminescence behaviors (Fig. 5). As shown in Fig. 5a1, β-$NaYF_4$:0.20Yb^{3+}, 0.02Ho^{3+} nanorods showed dominant emission peaks at 539 and 645 nm, which were assigned to the $^5S_2/^5F_4 \rightarrow {}^5I_8$ and $^5F_5 \rightarrow {}^5I_8$ transitions of Ho^{3+} ions, respectively.[31] For β-$NaYbF_4$:0.02Er^{3+}, three emission bands centered at 519, 538 and 654 nm were observed (Fig. 5a2), which were assigned to $^2H_{11/2} \rightarrow {}^4I_{15/2}$, $^4S_{3/2} \rightarrow {}^4I_{15/2}$ and $^4F_{9/2} \rightarrow {}^4I_{15/2}$ transitions of Er^{3+}, respectively.[32] Among them, the red emission was remarkably significant. A faint peak attributed to $^2H_{9/2} \rightarrow {}^4I_{15/2}$ transition at 407 nm was found, which is due to a three-photon process. The unique UC luminescence behavior of the as-synthesized β-$NaYF_4$:Yb^{3+}/Ho^{3+}@β-$NaYbF_4$:Er^{3+} core/shell nanorod sample (Q5) is shown in Fig. 5a3. The typical emissions of Ho^{3+} and Er^{3+} co-existed in the sample. The emission bands at 519 and 653 nm corresponded to $^2H_{11/2} \rightarrow {}^4I_{15/2}$ and $^4F_{9/2} \rightarrow {}^4I_{15/2}$ transitions of Er^{3+}, while the main band at 539 nm and a shoulder at 641 nm were attributed to $^5S_2/^5F_4 \rightarrow {}^5I_8$ and $^5F_5 \rightarrow {}^5I_8$ transitions of Ho^{3+}, respectively. Two additional bands at 750 and 807 nm correspond to $^5S_2/^5F_4$–$^5I_7$ transitions of Ho^{3+} and $^4I_{9/2} \rightarrow {}^4I_{15/2}$ transitions of Er^{3+}, respectively.

Second, the shell thickness has a great effect on the UC emission. Fig. 5b displays the UC emission spectra of β-$NaYF_4$:0.20Yb^{3+}, 0.02Ho^{3+}@β-$NaYbF_4$:0.02Er^{3+} (from Q1 to Q5 sample with different amounts of each precursor) under 980 nm laser excitation. It can be seen that the emission intensities of both Er^{3+} and Ho^{3+} increase monotonically with increasing content of the precursor, *i.e.*, the entire emission is enhanced with the shell coating. This results from surface passivation effects.[8,33,34] The enhanced intensity of Er^{3+} was attributed to the increased content of precursor. From the corresponding luminescence photographs, as shown in Fig. 5c, we know that the successive adjustment of color output can be readily achieved by controlling the shell thickness, *i.e.* the volume of the precursory α-$NaYbF_4$:Er^{3+} colloid solution.

Third, based on the epitaxial growth-induced phase transformation from cubic α-phase in solution to hexagonal β-one on the shell structure, the enhancement of optical performance of β-$NaYF_4$:0.20Yb^{3+}, 0.02Ho^{3+} and β-$NaYbF_4$:0.02Er^{3+} (Fig. S3†) as respective cores can also be suggested by growing an optical inert β-$NaYF_4$ material as the shell. The XRD and TEM image of α-$NaYF_4$ precursor are shown in Fig. S4.† After epitaxial growth, the phase purity of P and R samples were confirmed by XRD, and the results are displayed in Fig. S5 and S6,† respectively. As shown in Fig. 6, the UC emission intensities of Ho^{3+} and Er^{3+} increase monotonically along with the increase of the content of α-$NaYF_4$ as the precursor of the β-$NaYF_4$ shell under our experimental condition. As considered previously,[35] the simple mixture of optically active β-$NaYF_4$:Yb^{3+}/Er^{3+} and optically inert undoped $NaYF_4$ would reduce the initial UC emission intensity of the optically active material. Herein, great enhancement of UC luminescence can be achieved, reflecting the surface passivation effect of the optically inert $NaYF_4$ shell coating on β-$NaYF_4$:0.20Yb^{3+}, 0.02Ho^{3+} and β-$NaYbF_4$:0.02Er^{3+} more intuitively (Fig. 6). The corresponding element mappings of Yb^{3+} and Y^{3+} for P5 and R5 (Fig. S7 and S8†) further confirm the core/shell

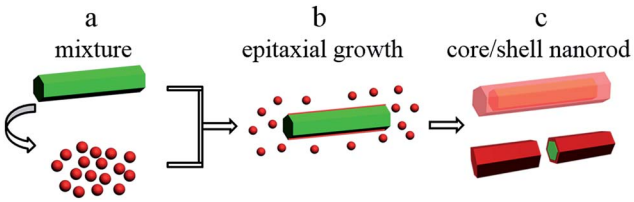

Scheme 1 Illustration of the formation of hexagonal β-$NaYF_4$:Yb^{3+}/Ho^{3+}@β-$NaYbF_4$:Er^{3+} core/shell nanorods.

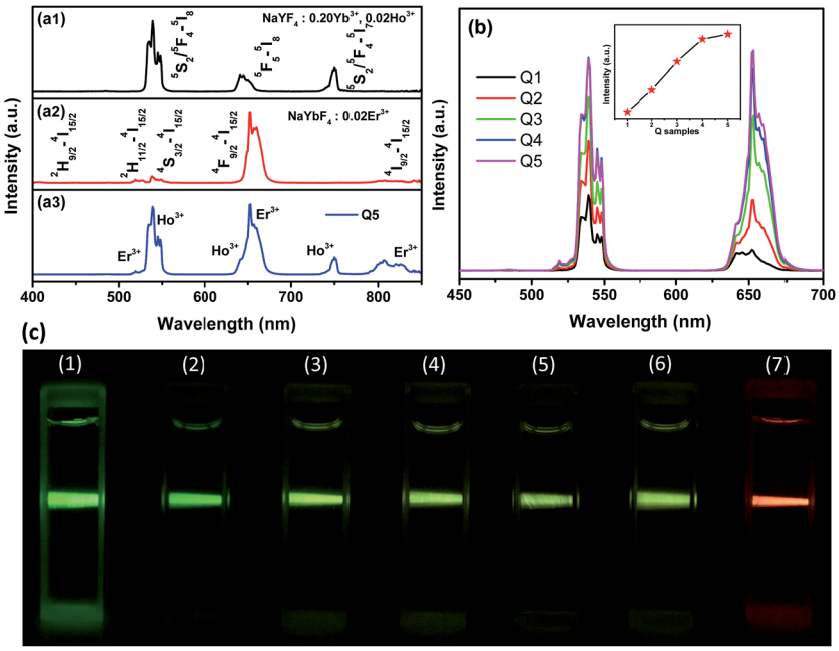

Fig. 5 UC spectra of (a1) β-$NaYF_4$:0.20Yb^{3+}, 0.02Ho^{3+}, (a2) β-$NaYbF_4$:0.02Er^{3+}, (a3) Q5, (b) Q1–Q5 samples under 980 nm laser excitation (0.2 W mm^{-2}) at RT. (c) Corresponding luminescence photographs of the samples re-dispersion into PEG 200 under 980 nm laser excitation, samples no. 1–7 are β-$NaYF_4$:0.20Yb^{3+}, 0.02Ho^{3+}, Q1, Q2, Q3, Q4, Q5, and β-$NaYbF_4$:0.02Er^{3+}, respectively.

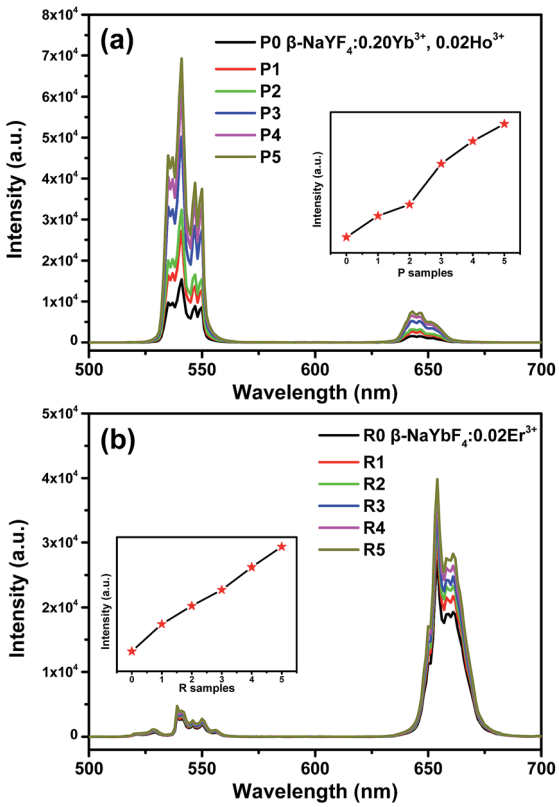

Fig. 6 UC emission spectra of P0–P5 and R0–R5 under 980 nm laser excitation at RT.

architecture. Therefore, our proposed procedure for the core/shell nanostructure based on the epitaxial growth and the epitaxial growth-induced phase transformation may be a versatile route to realize optical enhancement and tailoring.

4. Conclusions

We synthesized β-$NaYF_4$:Yb^{3+}/Ho^{3+}@β-$NaYbF_4$:Er^{3+} shell-active core/shell nanorods *via* a facile hydrothermal method. The phase, morphology, structure of α-phase precursor and β-phase nanorod template were confirmed by XRD, SEM and TEM. The different distributions of Yb^{3+} and Y^{3+} in the elemental mappings and line scan analyses proved the formation of core/shell architecture. UC luminescence enhancement was observed for β-$NaYF_4$:Yb^{3+}/Ho^{3+} after growing β-$NaYbF_4$:Er^{3+} shell. In addition, the improved UC emission of β-$NaYF_4$:Yb^{3+}/Ho^{3+} and β-$NaYbF_4$:Er^{3+} after the $NaYF_4$ coating further confirms the surface passivation effect. Tailored UC emissions could be obtained by controlling the shell components and thickness in β-$NaYF_4$:Yb^{3+}/Ho^{3+}@β-$NaYbF_4$:Er^{3+} core/shell nanorods. The tunable colors with improved emission in these core/shell nanorods may find wider potential applications in multicolor labeling and anti-counterfeiting.

Acknowledgements

This study was financially supported by grants from the Joint Funds of the National Natural Science Foundation of China and Guangdong Province (No. U1301242), Research Fund for the Doctoral Program of Higher Education of China (RFDP) (No. 20130171130001), the National Natural Science Foundation of

China (51672315, 21271190) and Guangdong Province (No. 2016A030313305), Special Fund of Guangdong Province Project for Applied Science and Technology Research and Development (No. 2016B090931007, 2015B090927002, 2013A090100010 and 2012B091000026), the Science and Technology research general project of Guangzhou (Grant No. 201607010360).

Notes and references

1 M. Quintanilla, F. Q. Ren, D. L. Ma and F. Vetrone, *ACS Photonics*, 2014, **1**, 662–669.
2 Q. Q. Su, S. Y. Han, X. J. Xie, H. M. Zhu, H. Y. Chen, C.-K. Chen, R.-S. Liu, X. Y. Chen, F. Wang and X. G. Liu, *J. Am. Chem. Soc.*, 2012, **134**, 20849–20857.
3 J. P. Yang, Y. H. Deng, Q. L. Wu, J. Zhou, H. F. Bao, Q. Li, F. Zhang, F. Y. Li, B. Tu and D. Y. Zhao, *Langmuir*, 2010, **26**, 8850–8856.
4 Z. Chen, W. Zheng, P. Huang, D. T. Tu, S. Y. Zhou, M. D. Huang and X. Y. Chen, *Nanoscale*, 2015, **7**, 4274–4290.
5 X. Xu, Z. Wang, P. P. Lei, Y. N. Yu, S. Yao, S. Y. Song, X. L. Liu, Y. Su, L. L. Dong, J. Feng and H. J. Zhang, *ACS Appl. Mater. Interfaces*, 2015, **7**, 20813–20819.
6 S. H. Zheng, W. B. Chen, D. Z. Tan, J. J. Zhou, Q. B. Guo, W. Jiang, C. Xu, X. F. Liu and J. R. Qiu, *Nanoscale*, 2014, **6**, 5675–5679.
7 F. Wang, R. R. Deng, J. Wang, Q. X. Wang, Y. Han, H. M. Zhu, X. Y. Chen and X. G. Liu, *Nat. Mater.*, 2011, **10**, 968–973.
8 F. Wang, J. Wang and X. G. Liu, *Angew. Chem., Int. Ed.*, 2010, **49**, 7456–7460.
9 H.-Q. Wang and T. Nann, *ACS Nano*, 2009, **3**, 3804–3808.
10 H. Zhang, Y. J. Li, I. A. Ivanov, Y. Q. Qu, Y. Huang and X. F. Duan, *Angew. Chem., Int. Ed.*, 2010, **49**, 2865–2868.
11 Z. Yin, H. Li, W. Xu, S. B. Cui, D. L. Zhou, X. Chen, Y. S. Zhu, G. S. Qin and H. W. Song, *Adv. Mater.*, 2016, **28**, 2518–2525.
12 H. Dong, L.-D. Sun, Y. F. Wang, J.-W. Xiao, D. T. Tu, X. Y. Chen and C.-H. Yan, *J. Mater. Chem. C*, 2016, **4**, 4186–4192.
13 Y. L. Dai, H. H. Xiao, J. H. Liu, Q. H. Yuan, P. A. Ma, D. M. Yang, C. X. Li, Z. Y. Cheng, Z. Y. Hou, P. P. Yang and J. Lin, *J. Am. Chem. Soc.*, 2013, **135**, 18920–18929.
14 H. H. Gorris and O. S. Wolfbeis, *Angew. Chem., Int. Ed.*, 2013, **52**, 3584–3600.
15 M. Haase and H. Schäfer, *Angew. Chem., Int. Ed.*, 2011, **50**, 5808–5829.
16 Y. H. Zhang, L. X. Zhang, R. R. Deng, J. Tian, Y. Zong, D. Y. Jin and X. G. Liu, *J. Am. Chem. Soc.*, 2014, **136**, 4893–4896.
17 H. Zhang, Y. J. Li, Y. C. Lin, Y. Huang and X. F. Duan, *Nanoscale*, 2011, **3**, 963–966.
18 M. L. Deng and L. Y. Wang, *Nano Res.*, 2014, **7**, 782–793.
19 L. M. Wang, X. Y. Li, Z. Q. Li, W. S. Chu, R. F. Li, K. Lin, H. S. Qian, Y. Wang, C. F. Wu, J. Li, D. T. Tu, Q. Zhang, L. Song, J. Jiang, X. Y. Chen, Y. Luo, Y. Xie and Y. J. Xiong, *Adv. Mater.*, 2015, **27**, 5528–5533.
20 H. Dong, L.-D. Sun, Y.-F. Wang, J. Ke, R. Si, J.-W. Xiao, G.-M. Lyu, S. Shi and C.-H. Yan, *J. Am. Chem. Soc.*, 2015, **137**, 6569–6576.
21 Y. Sun, X. J. Zhu, J. J. Peng and F. Y. Li, *ACS Nano*, 2013, **7**, 11290–11300.
22 Y.-F. Wang, G.-Y. Liu, L.-D. Sun, J.-W. Xiao, J.-C. Zhou and C.-H. Yan, *ACS Nano*, 2013, **7**, 7200–7206.
23 C. Zhang, L. Yang, J. Zhao, B. H. Liu, M.-Y. Han and Z. P. Zhang, *Angew. Chem., Int. Ed.*, 2015, **54**, 11531–11535.
24 K. A. Abel, J.-C. Boyer, C. M. Andrei and F. C. J. M. van Veggel, *J. Phys. Chem. Lett.*, 2011, **2**, 185–189.
25 B. Chen, D. F. Peng, X. Chen, X. S. Qiao, X. P. Fan and F. Wang, *Angew. Chem., Int. Ed.*, 2015, **54**, 12788–12790.
26 S. Ye, G. Y. Chen, W. Shao, J. L. Qu and P. N. Prasad, *Nanoscale*, 2015, **7**, 3976–3984.
27 C. X. Li and J. Lin, *J. Mater. Chem.*, 2010, **20**, 6831–6847.
28 S. L. Gai, C. X. Li, P. P. Yang and J. Lin, *Chem. Rev.*, 2014, **114**, 2343–2389.
29 Y. W. Zhang and Z. L. Hong, *Nanoscale*, 2013, **5**, 8930–8933.
30 Y. H. Zhang, L. Huang and X. G. Liu, *Angew. Chem., Int. Ed.*, 2016, **55**, 5718–5722.
31 W. Gao, H. R. Zheng, Q. Y. Han, E. J. He, F. Q. Gao and R. B. Wang, *J. Mater. Chem. C*, 2014, **2**, 5327–5334.
32 M. Y. Ding, D. Q. Chen, S. L. Yin, Z. G. Ji, J. S. Zhong, Y. R. Ni, C. H. Lu and Z. Z. Xu, *Sci. Rep.*, 2015, **5**, 12745.
33 X. Y. Huang and J. Lin, *J. Mater. Chem. C*, 2015, **3**, 7652–7657.
34 D. M. Liu, X. X. Xu, F. Wang, J. J. Zhou, C. Mi, L. X. Zhang, Y. Q. Lu, C. S. Ma, E. Goldys, J. Lin and D. Y. Jin, *J. Mater. Chem. C*, 2016, **4**, 9227–9234.
35 T. Rinkel, A. N. Raj, S. Dühnen and M. Haase, *Angew. Chem., Int. Ed.*, 2016, **55**, 1164–1167.